Science of the Total Environment 649 (2019) 1338–1348

Contents lists available at ScienceDirect

Science of the Total Environment

journal homepage: www.elsevier.com/locate/scitotenv

Spatiotemporal impact of soil moisture on air temperature across the Tibet Plateau

Keke Fan [a,b,c], Qiang Zhang [a,b,c,*], Vijay P. Singh [d], Peng Sun [e], Changqing Song [a,b,c], Xiudi Zhu [a,b,c], Huiqian Yu [a,b,c], Zexi Shen [a,b,c]

[a] Key Laboratory of Environmental Change and Natural Disaster, Ministry of Education, Beijing Normal University, Beijing 100875, China
[b] Faculty of Geographical Science, Academy of Disaster Reduction and Emergency Management, Ministry of Education/Ministry of Civil Affairs, Beijing Normal University, Beijing 100875, China
[c] State Key Laboratory of Earth Surface Processes and Resources Ecology, Beijing Normal University, Beijing 100875, China
[d] Department of Biological and Agricultural Engineering and Zachry, Department of Civil Engineering, Texas A&M University, College Station, TX, USA
[e] College of Territorial Resource and Tourism, Anhui Normal University, Anhui 241002, China

HIGHLIGHTS

- New finding about impacts of soil moisture on near-surface air temperature via evaporation fraction.
- Identification of different response regimes via relations between soil moisture and evaporation fraction;
- Rigorous data preprocessing to reduce uncertainty in results.

GRAPHICAL ABSTRACT

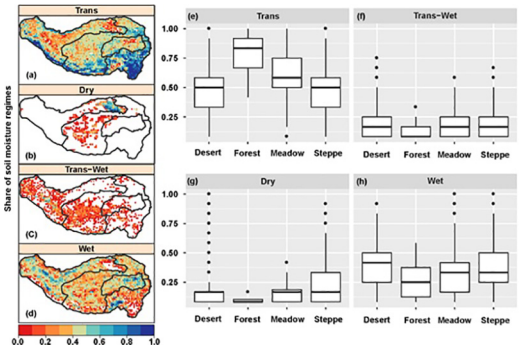

ARTICLE INFO

Article history:
Received 20 June 2018
Received in revised form 27 August 2018
Accepted 28 August 2018
Available online 28 August 2018

Editor: Jay Gan

Keywords:
The Himalayan Tibetan Plateau
Soil moisture
Air temperature
Evaporation fraction
Coupling between temperature and SM

ABSTRACT

The Himalayan Tibet Plateau (HTP) is regarded as the third pole of the globe and is highly sensitive to global climate change. The hydrothermal properties of HTP greatly impacts the water cycle of the HTP and climate change in its surrounding regions. Using the NCEP-CFSR dataset, this study investigated the spatiotemporal pattern of soil moisture (SM) during different seasons considering vegetation types. The response of the evaporation fraction (EF) to SM and the impact of SM on air temperature through evapotranspiration were analyzed. Results showed that the spatial distribution of SM across the HTP was persistent during different seasons. A decreasing SM trend was observed from southeastern to northwestern HTP. Further, results of this study indicated a wetting tendency in past thirty years, espcially in desert region. In addition, the majority of the HTP regions were dominated by persistent transitional SM conditions which could be identified in the Himalayas and the southeastern HTP, whereas a persistent SM deficit in the Qaidam basin. The sensitivity of temperature response to EF was the strongest during spring and summer. Moreover, the spatial distribution of sensitivity was highly consistent with the vegetation regionalization, indicating the remarkable impact of vegetation type on the sensitivity of temperature to EF changes in summer.

© 2018 Elsevier B.V. All rights reserved.

* Corresponding author at: Key Laboratory of Environmental Changes and Natural Hazards, Ministry of Education, Academy of Hazard Reduction and Emergency Management, State Key Laboratory of Earth Surface Processes and Resource Ecology, Beijing Normal University, Beijing 100875, China.
E-mail address: zhangq68@bnu.edu.cn (Q. Zhang).

https://doi.org/10.1016/j.scitotenv.2018.08.399
0048-9697/© 2018 Elsevier B.V. All rights reserved.

1. Introduction

Land-atmosphere interactions play a critical role in the climate system (Seneviratne et al., 2010), particularly in transitional climate regions (Guillod et al., 2015), where soil moisture potentially modifies the partitioning of energy available at the land surface into sensible and latent heat fluxes (Koster et al., 2004; Guillod et al., 2015). Meanwhile, soil moisture (SM) is also recognized as a vital variable controlling and adjusting surface runoff, soil drainage, and soil-freeze-thaw status (Seneviratne et al., 2010; Zhang et al., 2015), and also for numerical weather prediction and climate projections (Albergel et al., 2013). It is well acknowledged that SM acts as the interface (or connection) between land and atmosphere and is an important part of the Earth ecosystem. SM influences the net radiant flux, sensible and latent heat fluxes, ground surface air temperature, humidity, atmospheric circulation and precipitation, and stability of the atmospheric boundary layer. Soil moisture changes further enhance the complexity of land-air interactions and hence play a crucial role in climate change (e.g. Seneviratne et al., 2006). Thus, SM is highly valued by the Global Climate Observing System (GCOS) Programme which endorses it as an Essential Climate Variable (ECV) (Albergel et al., 2013).

Due to the modification of partitioning of the incoming energy into latent and sensible heat fluxes as a result of SM variations, SM directly influences climate processes, such as air temperature (Zhou and Geerts, 2013; Berg et al., 2014), boundary-layer stability, and precipitation (Taylor et al., 2012). SM can drive surface temperature changes by influencing the partitioning of the surface net radiation available into the latent heat flux and sensible heat flux (e.g. Hauser et al., 2016). Given sufficient SM, latent heat is limited by radiation; On the contrary, latent heat is limited by the SM availability under drought conditions. In this case, soil moisture deficit tends to decrease latent heat and hence increase sensible heat and consequently increase surface air temperature (Hauser et al., 2016). Actually, numerous observations have indicated relations between precipitation deficit, summer temperature, and hot extremes in many regions of the world (Hirschi et al., 2011; Mueller and Seneviratne, 2012; Zhang et al., 2015; Hauser et al., 2016) and a negative relationship between preceding SM conditions and summer monthly maximum temperature in Europe (Whan et al., 2015). In particular, impacts of SM deficit on droughts and heat wave temperatures have been of remarkable concern in recent years (Hirschi et al., 2011; Mueller and Seneviratne, 2012; Miralles et al., 2014; Hauser et al., 2016). However, numerous scientific issues are still unanswered in an integrated way. Therefore, it is necessary to revisit this issue, especially over the Tibet Plateau.

The Himalayan Tibetan Plateau (HTP) (Fig. 1) is well known as the Third Pole (Zhang et al., 2013) and the "roof of the world," with an average elevation of over 4000 m above mean sea level (a.m.s.l.). The HTP is also acknowledged as the "Asian Water Tower" supplying water resources for a range of major Asian rivers, such as Brahmaputra (Yaluzangbu), Salween (Nu), Mekong (Lancang), Yellow, and Yangtze rivers (Zhang et al., 2013; Subin et al., 2013). These rivers supply water resources for hundreds of millions of people living downstream (Zhang et al., 2013). Recent studies have found a warming tendency over the HTP (Xu et al., 2008; Xie et al., 2010) well above the global mean (IPCC, 2007). Warming climate has the potential to enhance evapotranspiration and enhanced transpiration has the potential to amplify SM deficit and hence SM deficit-induced partitioning of the energy available at the land surface into sensible and latent heat fluxes. It is a complicated SM-atmosphere feedback. Further, warming-induced aridity and decreased snowfall were observed in recent years (Gao et al., 2015; Deng et al., 2017). Hence, it is important to reflect on relations between SM and air surface temperature.

The above discussion indicates that the estimation of SM over the HTP has been emphasized in recent years (e.g. Chen et al., 2013; Bi et al., 2016). Schwingshackl et al. (2017) has proposed a simple framework to quantify the effect of spatial and temporal variations of soil moisture on air temperature in the world, but the coarse spatial scale cannot accurately represent the soil moisture control on air temperature at a smaller spatial scale. Few reports seem too have addressed the impact of SM on air surface temperature over the Tibetan Plateau, which is one of the regions' most sensitive to climate change. An answer of this issue can help shed a new light on the SM-atmosphere interactions over the HTP and related impacts on the hydrological cycle over the HTP as well as climate change in the surrounding regions. This study therefore. The objective of this study therefore investigates the relation between SM and evapotranspiration and temperature over the HTP and the SM-temperature coupling over the HTP in both space and time and identify relevant driving factors, such as vegetation cover and evapotranspiration. This study is a typical regional scale study on the SM-atmosphere interactions over the HTP which is most sensitive to global climate change.

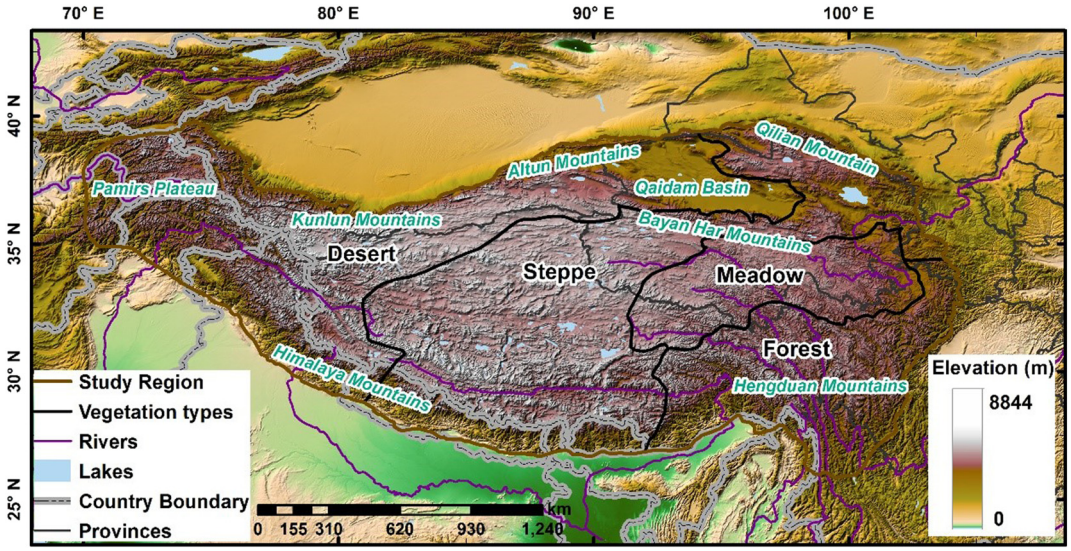

Fig. 1. The vegetation regionalization over the Tibetan Plateau.

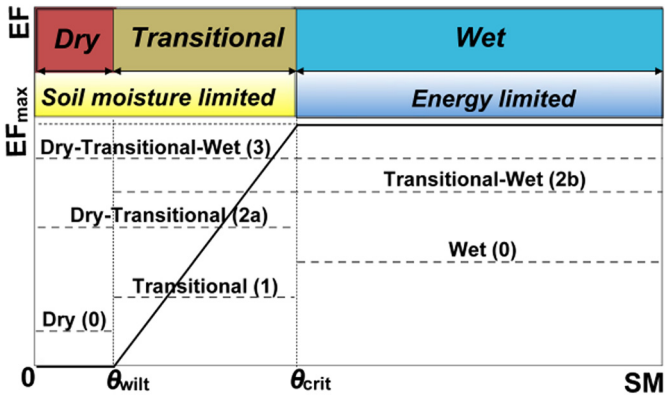

Fig. 2. The relation between evaporative fraction and soil moisture under different values of soil moisture availability. This figure is revised after Seneviratne et al. (2010).

2. Study region and the dataset

The HTP is located between 25°N–40°N and 70°E–105°E (Fig. 1). Based on the vegetation atlas of China with a scale of 1:1000000, the entire HTP was regionalized into nine vegetation zones according to the vegetation zone from Chinese Academy of Sciences (Liu et al., 2016; Zhang et al., 2018b). Through integrating these zones, four large vegetation divisions can be obtained as forest, meadow, steppe, and desert (Fig. 1). The data used in this study was the NCEP-CFSR (The National Centers for Environmental Prediction-Climate Forecast System Reanalysis) which was developed at the Environmental Modeling Center at NCEP. The CFS (Climate Forecast System) is a fully coupled model representing the interaction between the Earth's atmosphere, oceans, land and sea ice. It became operational at NCEP in March 2011 (http://cfs.ncep.noaa.gov/) (Saha et al., 2010; Saha et al., 2014). Previous studies estimated the NCEP-CFSR dataset and found that this dataset provided a relatively good estimation for many variables, and some studies were related to the Tibetan Plateau (Bao and Zhang, 2013; Feng et al., 2014; Liu et al., 2018; Zhao et al., 2018). Otherwise, the NCEP-CFSR dataset contains all possible variables which are necessary to conduct this study. Daily SM and maximum temperature for 1979–2010 with a spatial resolution of 0.3° × 0.3° were analyzed in this study. Four soil layers of SM were considered, i.e., 0–0.1 m, 0.1–0.4 m, 0.4–1 m, 1–2 m. SM of the upper three soil layers between 0 and 1 m was taken as the root-zone SM. Besides, upward/downward long-wave radiation, upward/downward shortwave radiation and latent/sensible heat flux were also analyzed and were obtained from this dataset.

3. Methods

Solar radiation is the main source of energy for the Earth. When it enters the atmosphere, it is reflected by clouds, the atmosphere, and the Earth surface and then returns into space. The net radiation on the

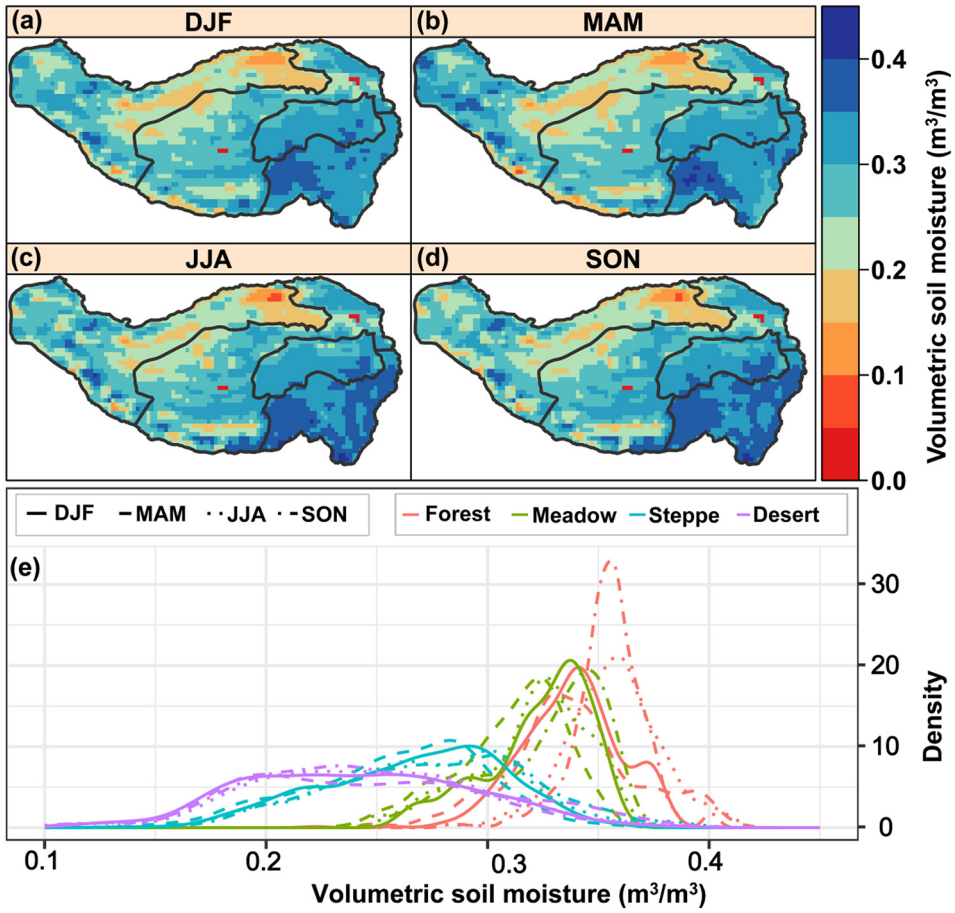

Fig. 3. The spatial distribution and probability density diagrams of soil moisture in different seasons: (a) December–February, (b) March–May, (c) June–August, (d) September–November. Each grid represents mean soil moisture data during 1979–2010. The color bar refers to the content of SM, and blue color represents high SM content, red color low SM content. In the bottom panel, the line types refer to different seasons and the colors represent different regions.

Earth surface reflects the energy balance at the Earth surface and can be quantified by the downward radiation flux and the upward radiation flux. The net radiation can be computed as:

$$Rn = Rds + Rdl – Rul – Rus \quad (1)$$

where Rn is the net solar radiation reaching the Earth surface; Rds denotes the downward shortwave radiation flux, and Rdl the downward long-wave radiation flux; Rul refers to the upward long-wave radiation flux, and Rus denotes the upward shortwave radiation flux.

The surface net radiation (Rn) transmits energy to the atmosphere through the evapotranspiration process and convective motions and to the ground through the soil conductivity. The energy balance equation can be expressed as:

$$Rn = LE + H + G \quad (2)$$

where LE refers to the latent heat flux; E denotes the evaporation or condensation mass flux; L denotes the energy change per unit weight of phase-changed water by evaporation or condensation, being about 2.5×10^6 J/kg; H is the sensible heat flux; and G is the soil heat flux.

SM affects atmospheric state through modifications of latent heat flux by evapotranspiration processes. Its SM variation alters the conversion ratio of net radiation to latent heat flux, sensible heat flux, and soil heat flux. The energy balance equation with consideration of energy conversion becomes:

$$LE/Rn + H/Rn = 1 - G/Rn \quad (3)$$

The term LE/Rn is taken as the evaporative fraction, or simply EF:

$$EF = LE/Rn \quad (4)$$

The following equation relates to different SM conditions:

$$EF(\theta) = \begin{cases} 0, & if\ \theta < \theta_{wilt} \\ EF_{\max}\dfrac{\theta - \theta_{wilt}}{\theta_{crit} - \theta_{wilt}}, & if\ \theta_{wilt} \le \theta \le \theta_{crit} \\ EF_{\max}, & if\ \theta > \theta_{crit} \end{cases} \quad (5)$$

where Q_{wilt} denotes the withering point of SM, and Q_{crit} denotes the critical SM value. Eq. (5) indicates different EF responses to SM variations under different SM conditions (Koster et al., 2009; Seneviratne et al., 2010; Schwingshackl et al., 2017) (Fig. 2). Based on Q_{wilt} and Q_{crit}, the $EF(\theta)$ function can be subdivided into three phases: (1) dry phase: the SM deficit can be observed given $\theta < \theta_{wilt}$ and EF is constrained by the availability of SM. In this phase SM is lower than Q_{wilt} and no water mass can be available for evaporation. Thus, given $\theta < \theta_{wilt}$, EF can be assumed to be 0. (2) Transitional phase: SM is in the transitional condition given $\theta_{wilt} < \theta < \theta_{crit}$. Under this condition, evaporation processes heavily depend on the availability of SM and hence the positive relations can be expected between EF and SM. If a linear relation can be assumed between EF and SM, the regions under this SM condition can be acknowledged with evident land-atmosphere coupling phenomenon. (3) Wet phase: given $\theta > \theta_{crit}$, sufficient SM can be expected and evapotranspiration processes are free of the availability of SM but are limited by the net solar radiation. In this case, SM is sufficient but nearly has no impact on evaporation processes. Θ_{wilt} is determined mainly by soil structure and soil texture, while θ_{crit} is controlled by the combined effect of soil struc-

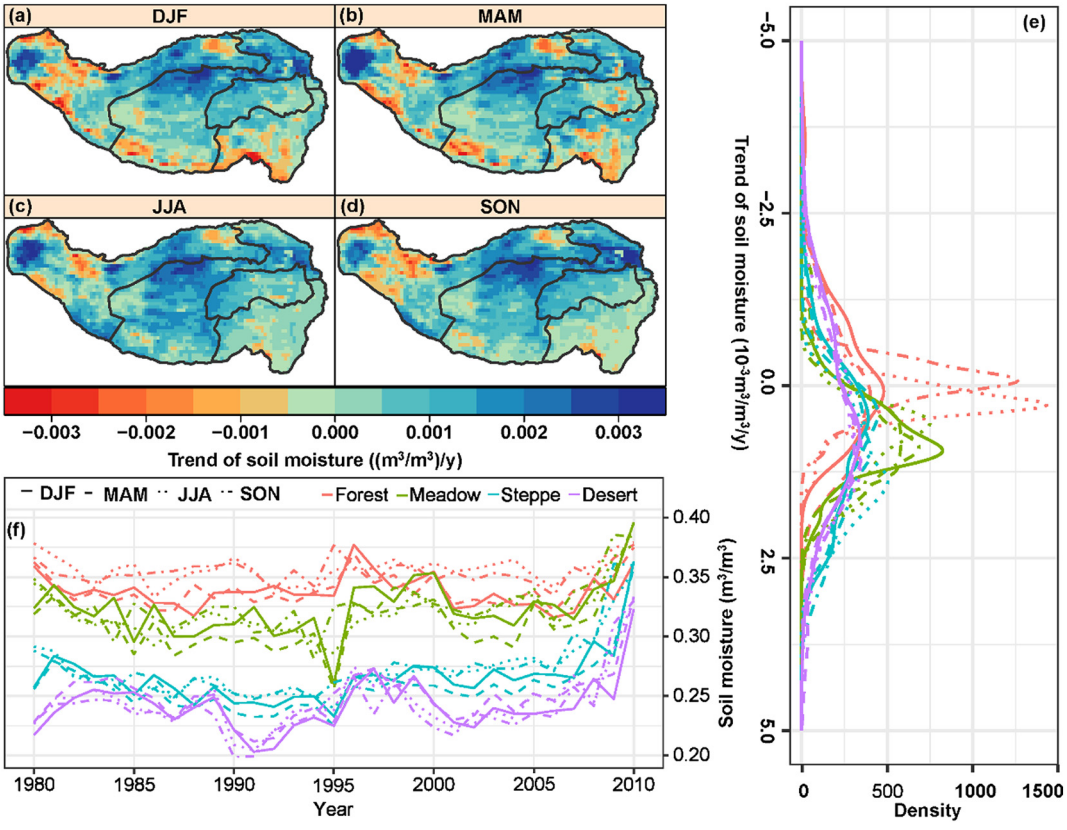

Fig. 4. The spatial distribution for the trend of soil moisture in different seasons: (a) December–February, (b) March–May, (c) June–August, (d) September–November. Each grid represents the trend of annual average SM during 1979–2010, derived from linear regression model by least square method. The color bar refers to the trend tof SM, and blue color represents increasing trend, red color decreasing trend. The other two figures are respectively probability density diagrams of the trend: (e) and the time series of annual average SM: (f) in the right and bottom panel, the line types refer to different seasons and the colors represent different regions.

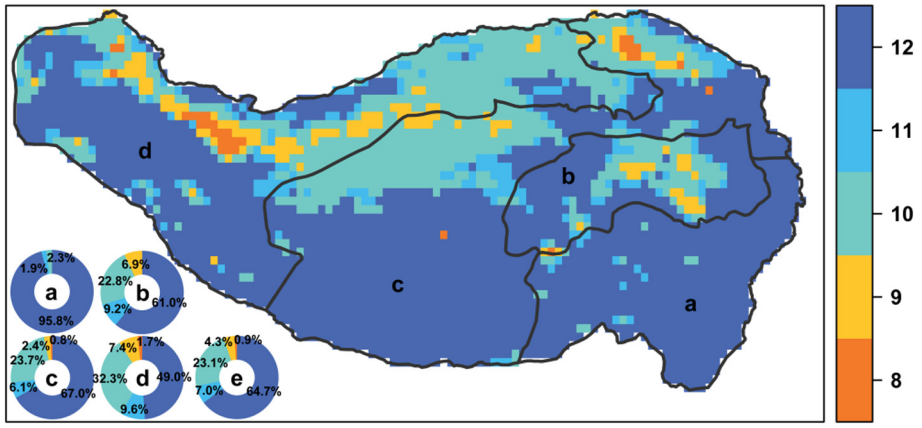

Fig. 5. Spatial distribution of number of considered 3-month subsets and the proportion of considered 3-month subsets within different subregions (a: forest; b: meadow; c: steppe; d: desert; and e for entire region). January to March, February to April, …, December to February were identified as 12 time intervals. The number just refers to the 3-month subsets with at least 25% valid data. The identification method has been presented in the Methods part.

ture, soil texture and net solar radiation. Specifically, the wet regime can be observed mainly in regions located in high latitude and/or in tropical regions (Schwingshackl et al., 2017).

Different relations between EF and SM are related to different SM conditions. Evaporation is near 0 when SM is lower than θ_{wilt}. In this case, EF is 0; when SM is higher than θ_{crit}, EF is constrained by energy and can reach EF_{max} due to sufficient SM; while linear relations between SM and EF can be expected given $\theta_{wilt} < SM < \theta_{crit}$. Therefore, relations between EF and SM under different SM conditions can be quantified by five models, i.e. model 0, model 1, model 2a, model 2b and model 3 (Fig. 2, Schwingshackl et al., 2017).

Schwingshackl et al. (2017) argued that evaporative fraction makes sense when all variables concerned are positive. Therefore, reliability and validity of the data should be checked and confirmed before further analysis. Pixels with negative values of latent and sensible heat, and net radiation were removed and the EF value should satisfy $0 \le EF \le 1$ (Schwingshackl et al., 2017). In addition, the time scale of SM changes is usually multi-monthly and three months were taken as a time unit, so January to March, February to April, …, December to February were identified as 12 time intervals for further analysis to identify the relation between SM and EF. If one grid contains data with 75% of the missing values then this grid will not be used in analysis. Therefore, meaningful

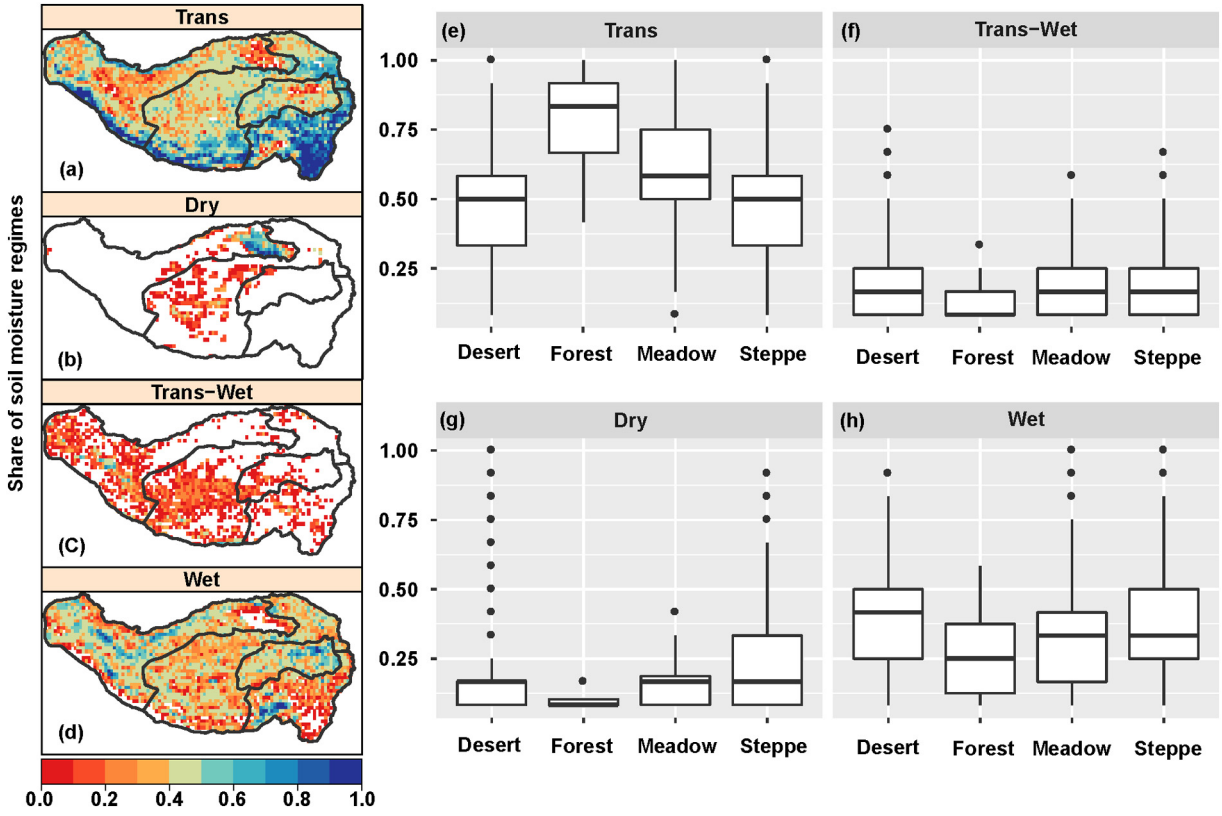

Fig. 6. The share of different soil moisture regimes and the box diagram of the share for four different regions. Only four kinds of regimes are considered: (a, e) transitional regime, (b, g) dry regime, (c, f) transitional and wet regime, (d, h) wet regime. The other two regimes, i.e., dry-transitional regime and dry-transitional-wet regime are not considered (Schwingshackl et al., 2017).

data grids were selected before subsequent analyses. Besides, cross validation method was used to determine the model for quantification of the relation between EF and SM and the detailed procedure can be found in Schwingshackl et al. (2017).

4. Results and discussion

4.1. Spatiotemporal distribution of SM changes across the HTP

The SM changes across the HTP are mainly affected by precipitation variations due to the Indian summer monsoon, and the melting of glaciers and permafrost over the HTP. Fig. 3 shows the spatial characteristics of seasonal SM changes on the HTP. In general, the spatial pattern of SM over the HTP during different seasons was consistent, showing a decreasing SM trend from southeastern to northwestern HTP (Zhang et al., 2018a), roughly in line with the route direction of the Indian summer monsoon, while lower SM was found in the Qaidam basin, and higher SM was observed in northwestern and northeastern HTP when compared to the north. From the viewpoint of vegetation coverage, the spatial pattern of SM was in accord with that of vegetation types, and SM content was ordered respectively: forest > meadow > steppe > desert. From a time point of view, SM content differed largely from place to place in every season. There was no consistent conclusion for different regions. In the desert, the SM content varies slightly in different seasons. In the forest, higher SM, e.g. 0.36 m^3 m^{-3}, can be found in summer and autumn, but lower SM, e.g. 0.335m^3 m^{-3}, in winter and spring. The highest SM in the Qaidam basin was observed during spring and lower SM during summer, which can be attributed to higher evapotranspiration as a result of higher temperature during summer. Meanwhile, the water vapor flux cannot reach the Qaidam basin and limited water content input can be expected and hence lower SM during summer in the Qaidam basin. Seasonal shifts from winter to spring were characterized by higher air temperature and hence more melting water from glaciers and snow in the Qilian Mountain, Altun Mountain, and Bayan Hara Mountain, etc. Meanwhile, relatively lower temperature during winter in the Qaidam basin resulted in lower evapotranspiration. Therefore, the SM content in the Qaidam basin followed the order as: spring > winter > autumn > summer.

As for SM along the Himalayan Mountains, due to the melting of ice and snow as a result of increasing air temperature during spring relative to winter and due to low evapotranspiration as a result of relatively less radiation flux relative to summer, the highest SM content can be expected in spring, and SM during summer is mainly affected by precipitation and melting of ice and snow and evapotranspiration. The SM content followed the order as: spring > summer > autumn > winter. The probability density function map (Fig. 3e) was consistent with the spatial distribution of SM. Compared with SM of other regions, the SM in the forest regions was the highest with smaller variability, being 0.3–0.4 m^3/m^3. A larger SM variability was found in the meadows and steppes with a left shift of the probability distribution curve and a long light tail feature. The highest SM variability was found in the desert with flattened curve shape and no evident peak values. The apparent kurtosis was mainly due to the large spatial span in latitude and longitude in this region. The regional SM division depended not only on precipitation, but also on the regional temperature, such as in the western part of the Tibetan Plateau where the elevation is high and the temperature is low, and it is not suitable for vegetation growth. However, the SM content is relatively high. In the northern Tibetan Plateau, low

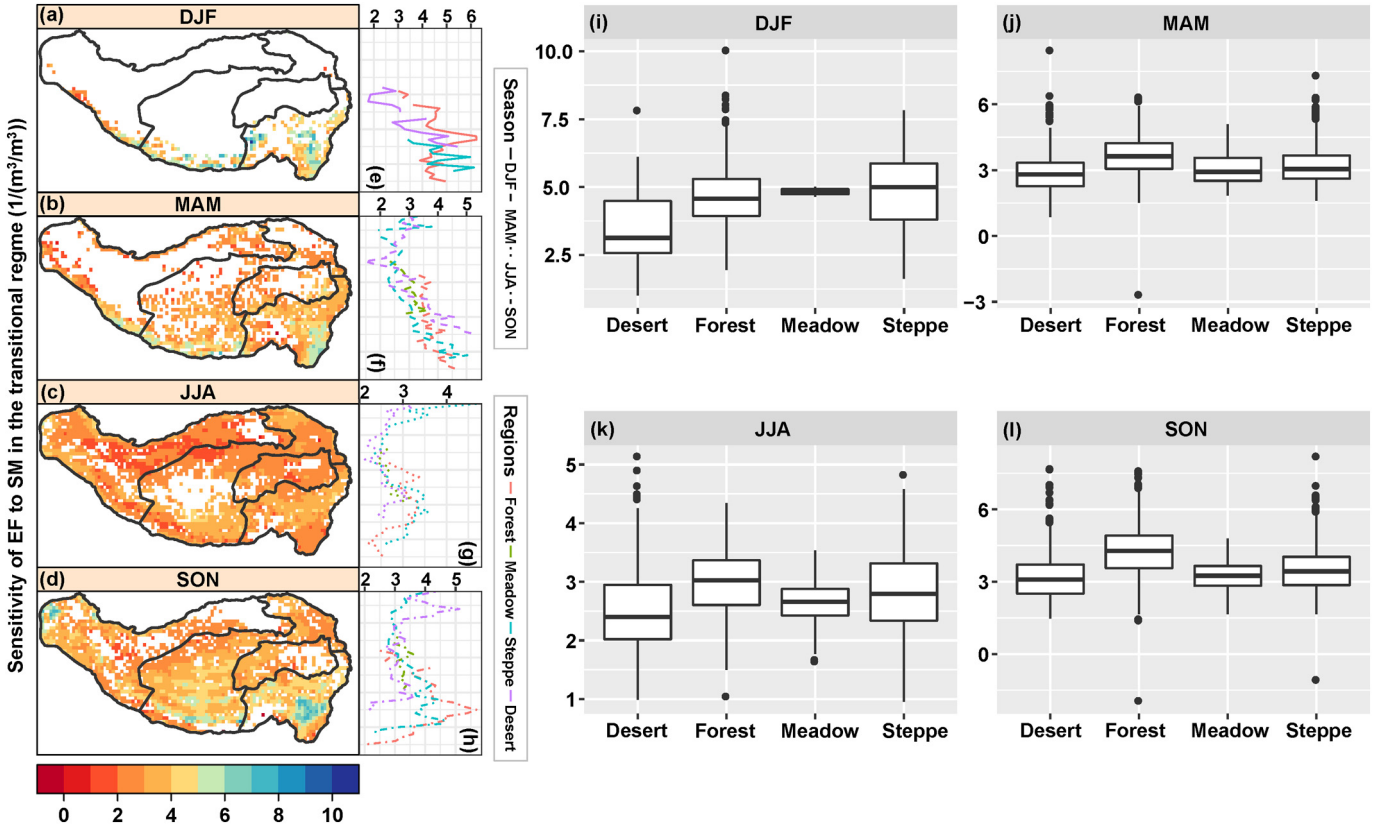

Fig. 7. The spatial distribution of response of evaporative fraction to soil moisture under the transitional regime in different seasons (a–d, the blank grid represents the regions without the transitional regime), the variation of response along with the latitude in different regions during different seasons (e–h, the line types refer to different seasons and the colors represent different regions) and the box diagram of response in different regions during different seasons (i–l, the line in the box is the median value, the box is the interquartile range, the vertical line endpoints are the 5th and 95th percentiles, and the points denote the outliers lying outside the 5th and 95th percentiles). DJF refers to December–February; MAM is March–May; JJA refers to June–August; SON is September–November.

precipitation and high evapotranspiration lead to low soil moisture, so no sufficient water supply is available for vegetation growth. Therefore, a larger SM variability was observed in the desert areas. With the exception of no evident seasonal SM variations in the desert, the SM content during autumn was the largest in other three regions. It was due to the large amount of precipitation in autumn and lower evapotranspiration as a result of the lower temperature during autumn. Therefore, the SM changes relied on precipitation at that time, but were also affected by ante-precipitation and other forms of water supply, such as melted snow.

Fig. 4 shows the spatial distribution of SM changes over the HTP during different seasons. Although SM changes were subjected to seasonality, a general drying tendency was observed over the western and southeastern HTP, but an increasing SM tendency was detected in the Pamirs with the largest increasing magnitude, implying increased SM content due to increased air temperature and the enhanced melting of the permafrost in the Pamirs. Relatively lower SM was found in the Qaidam basin and had a decreasing trend during all seasons. In the Himalayan Mountains, SM decreased during spring and winter, but increased during summer and autumn. This was likely due to spatial changes in precipitation. In general, the SM changes followed a spatial pattern, that is, SM on the Tibetan Plateau tended to be increasing, especially in the last decade. The probability distribution (Fig. 4e) was consistent with the spatial distribution of trends in SM. As a whole, with the exception of a slight decrease of SM during autumn in the forest regions, the SM content of the other three regions exhibited an overall upward trend. Besides, Fig. 3e shows that SM in the forest region during autumn was the largest. Meanwhile, the increase in the SM content was most obvious in the meadow region, and most areas were dominated by increasing SM trends. The increasing magnitude of SM in the desert region was the second largest with a large changing variability of $-2.0–2.5 \times 10^{-3}$ $m^3/m^3/y$ (Fig. 4e). The changing magnitude of SM in different regions followed the order as: desert > steppe > meadow > forest.

The SM changes in different years were significantly different, although SM in different regions of the HTP had an overall upward trend (Fig. 4f). In general, SM decreased at first and was followed by an increase, and then the decrease of SM was followed by a sharp increase. However, this changing pattern was slightly different in different regions. In the forest area, the SM content was the highest with a small changing SM variability. In the meadow area, SM had a downward trend from 1980 to 1995, and had an increasing tendency after 1995 till 2000, and then was followed by a slight decrease. SM in the meadow region was subject to a larger changing variability. In the steppe area, SM had a slight downward trend in 1995 and then had a gradual increase. In desert areas, SM first increased until 1983, then decreased up to 1987 and was followed by a low trough SM value in 1991 and 1995 respectively. The consistent trough values appeared in 1995 within four different regions, implying abnormally insufficient precipitation amount in 1995 over the whole Tibet Plateau. Meanwhile, SM tended to increase after 2003 and after 2005 in particular. This increased SM after 2003 can be attributed to a persistent increase in precipitation and the increased melting of ice and snow.

4.2. Time intervals without missing SM

Time intervals with missing SM data accounting for 75% of the each data grid were excluded from analysis (Schwingshackl et al., 2017). Due to the high altitude of the HTP and relatively thin atmospheric layer, downward long-wave radiation from the atmosphere is relatively less, resulting in less net radiation than other regions at the same latitude. In particular, the net radiation and other radiative fluxes may be negative during the winter season. EF does make sense only if all the variables involved in Eq. (3) are positive, such as net radiation, latent heat flux, sensible heat flux, etc., and also these variables satisfy the condition of $0 < EF < 1$. Data points that don't satisfy the above-mentioned condition were excluded from analysis.

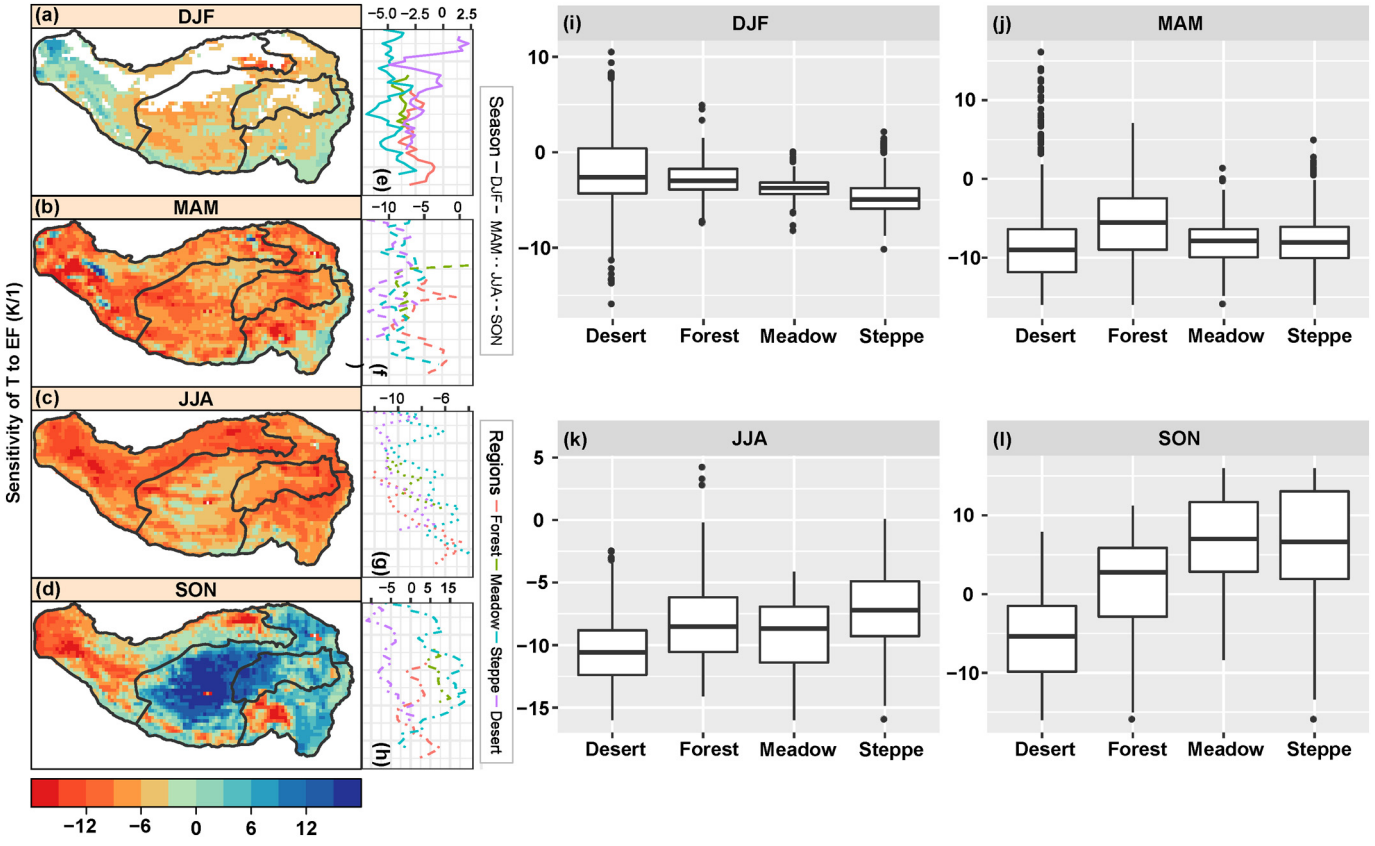

Fig. 8. Same as Fig. 7, but for the sensitivity of seasonal temperature responses to evaporative fraction in different seasons.

Fig. 5 shows the spatial distribution of the number of effective consecutive 3 months, i.e. 1st–3rd month, 2nd–4th month, ..., 12nd–2nd month, altogether 12 time intervals. It can be seen from Fig. 5 that the spatial pattern of the number of effective consecutive 3 months is subject to a clear latitudinal gradient and was in line with the results of Schwingshackl et al. (2017). The reanalysis dataset is more accurate in estimating the net radiation, sensible heat, and latent heat flux in low latitudes, and the estimation of these variables at higher latitude is subject to lower accuracy. The southern part of the HTP is located in the tropical and subtropical regions with stronger solar radiation. At the same time, due to the impact of the Indian monsoon, precipitation is large and evapotranspiration is significant. Therefore, the data of different months in most regions meet the requirements in further analyses of this current study. In the northern part of the HTP with higher latitude, less radiation flux and less significant evapotranspiration, few consecutive 3 months can be found with sufficient available data. Due to the presence of lakes, rivers, and other surface waters, as well as high elevation, only eight consecutive 3 months were available in parts of the northwestern part of the HTP (Kunlunshan) and the northeastern part of the HTP (Qilian Mountain). In addition, due to the influence of complex terrain and/or topographical features, such as Bayan Har Mountains, the estimation of flux was inaccurate and the data cannot meet the analysis requirements. Therefore, the effective number of the consecutive 3 months in the middle and eastern parts of the alpine meadow area had a trough value area.

4.3. Relationship between SM and EF

Three SM conditions were available, i.e. dry, transitional, and wet (Fig. 2). Schwingshackl et al. (2017) concluded that nearly no regions were found with the following conditions, i.e. dry-transitional, dry-transitional-wet conditions at the global scale, and the HTP is no exception. Therefore, in this study, the other four regimes except the above-mentioned conditions were analyzed (Fig. 6). Generally, the vast majority of the study area was in a transitional SM state during most of the time of the year. The southeastern part of the HTP belongs to a tropical climate with precipitation of >1000 mm and widespread rainforests as well. The SM content was sufficient along with abundant energy supply. Therefore, the θ_{crit} value was large and SM of the southeastern part of the HTP was in transitional conditions during the entire year. The same was for the SM in the Himalayas region, while the source of SM was precipitation and melting of ice and snow. The transitional-wet SM state was mainly in the middle latitudes of the HTP where the precipitation amount was moderate with sufficient SM content. Due to limited energy supply, the θ_{crit} value was relatively small. In the Qaidam basin, however, lower than 100 mm precipitation led to low SM content, being in long term dry SM conditions.

It can be seen from Fig. 6a that SM transitional conditions can be found mainly in forest regions. In other words, 80% of the time intervals considered were dominated by transitional SM conditions and then wet SM conditions, and during summer in particular. In the alpine meadow area, SM was in a transitional state during nearly 55% of the time, and

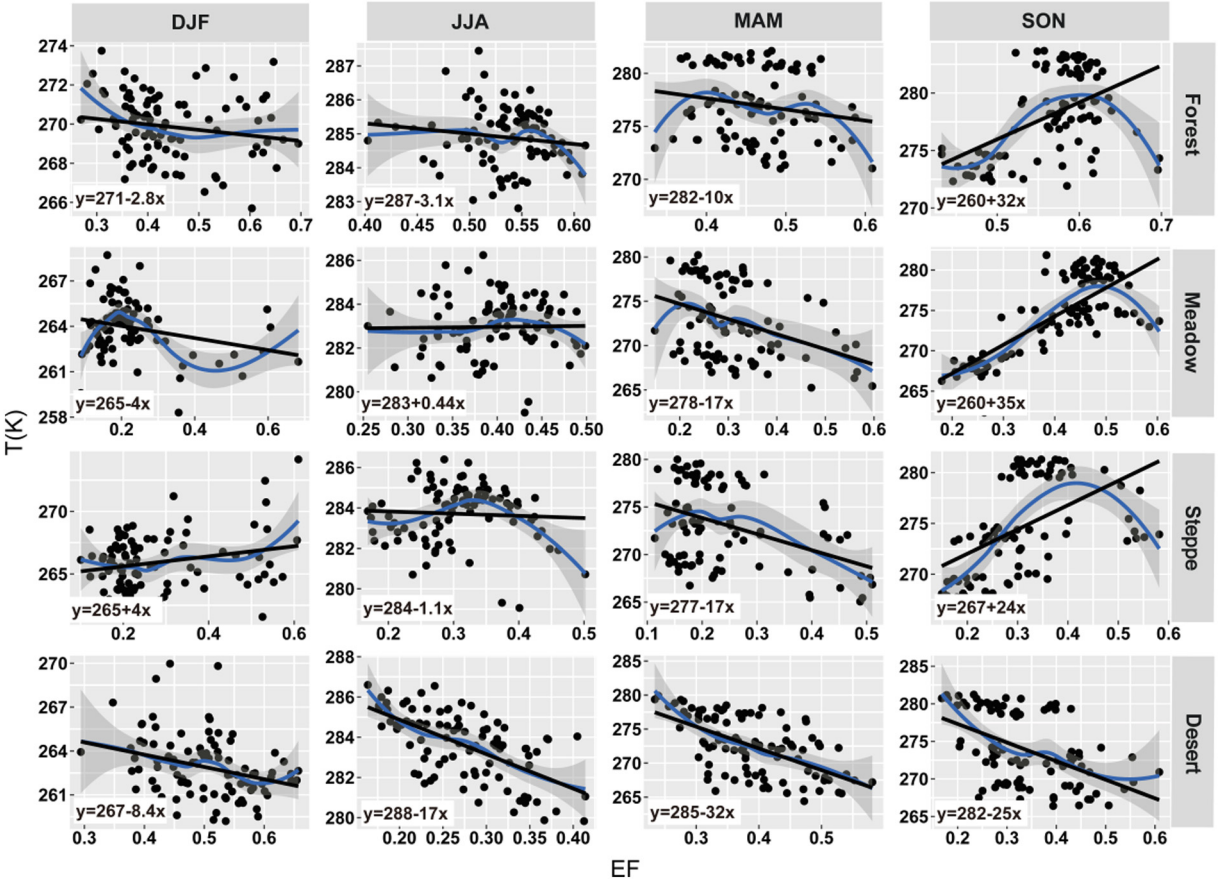

Fig. 9. Relations between temperature and evaporative fraction in diverse vegetation regions during different seasons. Four columns refer to four different seasons respectively: DJF (December–February); MAM (March–May); JJA (June–August); SON (September–November). Four rows refer to four different vegetation regions: Forest, Meadow, Steppe and Desert. Each point represents the corresponding annual average temperature and evaporative fraction in each vegetation region. The black straight line is the regression line by the ordinary least square method. The colored curve is fitted by the loess regression method. The shadow stripes refers to the 95% confidence interval.

was in a wet state during 30% of the time (Fig. 6a and c). In the alpine steppe area, different SM conditions were found throughout the year. Specifically, SM was in transitional state during half of the year and was followed by wet SM conditions. Different SM conditions corresponded to different vegetation coverage types. The percentage of the transitional SM state was different in different vegetation regions. The highest proportion of area with transitional SM condition can be found in forest regions, approximately 80%, followed by meadow, steppe, and desert regions (Fig. 6e). The percentage of areas with dry SM condition and transitional-wet SM condition was relatively low in all vegetation regions (Fig. 6f). The wet SM state was dominant in the desert area and was followed by steppes, meadows and forests (Fig. 6f). Meanwhile, the wet SM conditions were dominant in the desert region due to the fact that the northern part of HTP is at the higher latitude and the net solar radiation is small (Fig. 6d). Therefore, energy is the controlling factor for evapotranspiration. Thus, the value of θ_{crit} was lower. In addition, due to the melting of snow and ice from the Pamirs, Kunlun Mountains, Himalayas, higher SM content can be observed in the western part of the desert area.

4.4. EF response to SM changes

SM affects the spatial allocation and distribution of ground surface energy via evapotranspiration. Fig. 7 shows the response of EF to SM given the transitional SM state. In this study, analyses were done on EF responses to SM changes for regions with linear relations between SM and EF only. In winter, higher SM content can be found in the southern Himalayas and forest areas and SM was in a transitional condition (Fig. 7a). In spring and summer, the sensitivity of EF responses to SM had no evident spatial variability (Fig. 7b and c). In addition, in spring, with the increase of latitude, EF first decreased and then increased in response to SM (Fig. 7f); in summer, with the increase of latitude, the EF response to SM increased at first and then decreased, and increased again (Fig. 7g). In autumn, the effect of evapotranspiration on SM was distinctly different in space (Fig. 7h). The sensitivity of EF response to SM was higher in forest areas and in the northwestern part of the HTP. However, the causes behind similar sensitivity of the EF response to SM were different. In the northwestern HTP, higher temperature during summer and autumn, the melting of ice and snow during these seasons leads to higher SM content. In forest areas, abundant precipitation at this time causes higher SM content. At the same time, sufficient solar radiation can help provide enough energy for evapotranspiration. Except for winter, the sensitivity of EF response to SM in high latitude was not analyzed. In other seasons, it can be found that the sensitivity of EF response to SM increased at high latitudes. This is mainly attributed to the fact that ice, snow, and permafrost in the western HTP are highly affected by temperature variations. The response of spring EF to SM changes was subject to no evident spatial variability, indicating that different vegetation types had little effect on the sensitivity of EF response to SM due to low temperature at that time (Fig. 7b). EF was mainly influenced and restricted by surface air temperature, and SM was relatively abundant. Therefore, the sensitivity of EF response to SM was larger in different regions in winter (Fig. 7a). Due to considerable low temperature in winter, SM was mostly in non-transitional SM conditions. Therefore, larger uncertainty can be expected and no further analyses were done.

4.5. Responses of temperature to EF variations

It can be seen from Eq. (3) that a larger proportion of net radiation would be used for evapotranspiration given larger EF, since the soil heat flux was small and was ignored in the current study. Further, the smaller the sensible heat flux, the lower the surface air temperature. Hence, theoretically, EF had a negative relation with temperature. Fig. 8 shows the spatial distribution of the sensitivity of temperature response to EF during different seasons. During spring and summer,

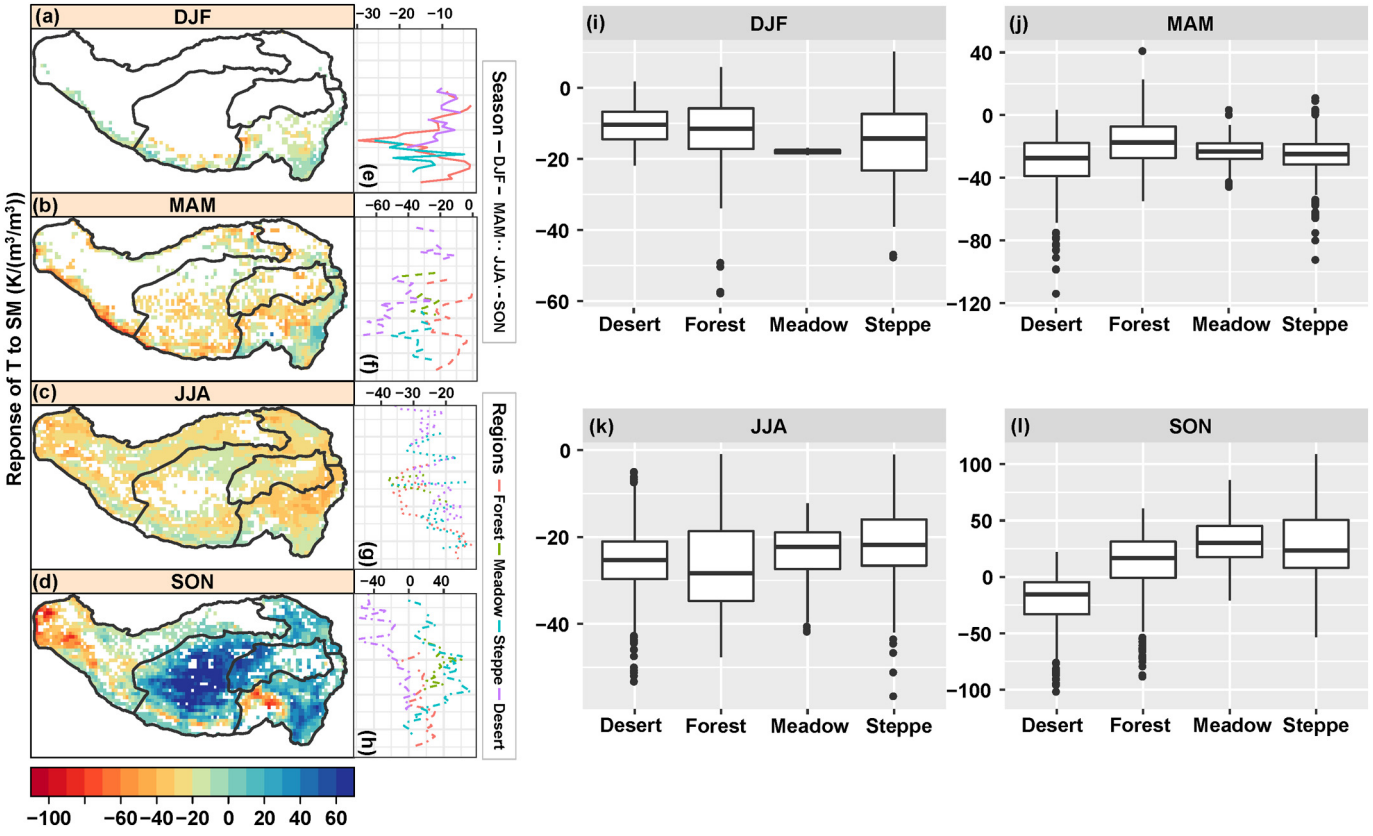

Fig. 10. Same as Fig. 7, but for responses of seasonal temperature to soil moisture under the transitional regime during different seasons.

temperature had a significant positive correlation with evapotranspiration on the whole. In winter, however, negative relations were dominant between temperature and evapotranspiration. In autumn, evident positive correlation was observed between temperature and evapotranspiration in the central and eastern Tibet Plateau. In summer, the spatial pattern of the sensitivity of temperature response to evapotranspiration was consistent with that of the vegetation zone across the HTP, indicating that the relationship between temperature and evapotranspiration was highly affected by vegetation conditions in summer.

The effect of temperature on evapotranspiration was shifting in different regions along different latitudes during different seasons. In winter, the relationship between temperature and evapotranspiration weakened with the increase of latitude in the desert area, and was subject to seasonal variability. In summer, enhanced relations between temperature and evapotranspiration were observed with the increase of latitude within the central and southern HTP dominated by different vegetation types. In the northern HTP, only desert and steppe coverage were available and weakened relationships were identified between temperature and evapotranspiration. In general, there were distinctly different temperature responses to evapotranspiration in regions with different vegetation types during different seasons, implying that the relationship between temperature and evapotranspiration was heavily affected by vegetation types, seasons, and latitudes. Besides, it can be seen from Fig. 8i–l that in winter, spring, and summer seasons, the sensitivity of temperature responses to evapotranspiration was negative. In winter, except for desert areas, the sensitivity of temperature response to evapotranspiration in other regions was positive. In desert areas, the highest sensitivity of temperature response to EF was observed in summer, being lower than −10, while in forest areas, the sensitivity of temperature response to evapotranspiration was the strongest in summer, being about −7. In meadows and steppe areas, the sensitivity of temperature response to evapotranspiration was the strongest in spring, being about −8.

It can be seen from Fig. 9 that temperature and EF were linearly related which can interpret the sensitivity of temperature response to EF to some extent. During spring season, weak sensitivity of temperature response to EF was identified in forest, steppe and meadow areas, especially in the meadow area, where the sensitivity was almost 0. In autumn, temperature was highly sensitive to EF in forest, steppe and meadow areas. Results from nonlinear fitting indicated persistently decreasing temperature with persistent increase of evapotranspiration in desert areas, while in forests and meadows, except for the winter season, temperature increased and then decreased with a persistent increase of EF. However, in winter, the response of temperature to EF was very different in different regions with different vegetation types.

4.6. Response of temperature to SM changes

Theoretically speaking, the higher the SM, the greater the EF, which in turn causes increased latent heat flux from net radiation for evapotranspiration. Correspondingly, the sensible heat flux decreases and the surface temperature decreases. In this case, the temperature decreases with the increase of SM (Schwingshackl et al., 2017). Except during autumn, SM had a significant negative feedback effect on temperature changes across the entire HTP (Fig. 10a, b and c); in autumn, however, except for desert areas, the temperature in most other regions increased with the increase of SM (Fig. 10d), which could be due to the uncertainty in datasets (Schwingshackl et al., 2017). In addition, due to the cumulative rainfall before autumn and increased precipitation during autumn, the SM content was abundant and exhibited little spatiotemporal variability. Temperature changes were mainly controlled by the energy availability, and hence weak response of temperature to SM (Fig. 8).

In spring, the sensitivity of temperature response to SM changes in the forest area was the lowest, which was mainly due to the uncertainty of the relationship between these two variables in forest regions. The sensitivity of temperature response to SM changes in other regions was between −20 and −40 K/(m^3/m^3). In summer, the sensitivity of temperature response to SM changes showed little spatial variability, ranging between −20 and −30 K/(m^3/m^3). Along the same latitude, the sensitivity of temperature to SM changes was subject to distinctly different spatial patterns, implying that vegetation types in different regions had a remarkable impact on the temperature response to SM changes and the sensitivity of temperature response to SM changes shifted along the latitude with different changing patterns for different seasons. In summer, the enhanced sensitivity of temperature response to SM changes was observed and the influence of different vegetation types on it was limited. This observation was attributed to the fact that summer season was dominated by abundant precipitation and higher temperature with high evapotranspiration. During winter, in desert areas, SM was mainly affected by the melting of ice and snow with no significant evapotranspiration, especially in the Pamirs in the northwestern HTP. Therefore, the relationship between temperature and SM tended to be weakened, while in other regions with different vegetation types, an enhanced relationship between temperature and SM was observed with the increase of latitude, because with the increase of latitude, the SM content decreased and the temperature change was constrained mainly by the availability of SM.

5. Conclusions

In this study, the NCEP-CFSR assimilation dataset was used to address the effect of SM on temperature variations in regions with different vegetation types. The impact of SM on EF variations through evapotranspiration processes was also investigated. The following findings can be drawn from this study:

(1) The spatial distribution of SM during different periods across the HTP are similar, i.e. SM is persistently decreasing from low to high latitude, and is decreasing from eastern to western HTP. In addition, SM across the HTP tend to become wetter, especially for desert region in the past decade. SM in the Qaidam basin is persistently decreasing during all seasons. SM in the Himalayan Mountains has a decreasing tendency during winter and spring seasons, and an increasing tendency during summer and autumn seasons.

(2) The transitional relationship can be identified between SM and EF across the vast majority of the HTP. Transitional relations between SM and EF along the Himalayas and the southeastern HTP are nearly all year around. Besides, the SM deficit can be observed in the Qaidam basin throughout the year. Moreover, transitional-wet SM conditions can be found mainly in the western HTP.

(3) High sensitivity of temperature responses to EF is negative in other regions than desert areas. During winter, lower sensitivity of temperature responses to EF can be identified. However, negative relations can be observed between temperature and SM during spring and summer. Particularly, during summer, the spatial pattern of high sensitivity of temperature responses to EF is highly consistent with that of vegetation regionalization across the HTP, implying that the relationship between temperature and SM is highly impacted by vegetation types.

(4) In winter, spring and summer, the humidity of the Tibetan Plateau has a significant negative feedback effect on the temperature change. Different regions have different responses to soil moisture changes in autumn, indicating that the uncertainty of temperature response to soil moisture in autumn is very uncertain. At the same latitude, the sensitivity of temperature to soil moisture varies greatly in different regions, indicating that different vegetation coverage has a significant effect on the relationship between the two. It fluctuates with the increase of latitude, and varies with the latitude in different seasons. There

are different trends with the change of latitude in different seasons.

Acknowledgments

This work is financially supported by the National Science Foundation for Distinguished Young Scholars of China, China (Grant No.: 51425903), the Fund for Creative Research Groups of National Natural Science Foundation of China, China (Grant No.: 41621061), and by National Natural Science Foundation of China (Nos. 41771536; 41601023). Our cordial gratitude should be extended to the editor, Prof. Dr. Jay Gan, and anonymous reviewers for their professional and pertinent comments and revision suggestions which are greatly helpful for further quality improvement of this manuscript.

References

Albergel, C., Dorigo, W., Reichle, R.H., Balsamo, G., Rosnay de, P., Muñoz-Sabater, J., Isaksen, L., Jeu de, R., Wagner, W., 2013. Skill and global trend analysis of soil moisture from reanalysis and microwave remote sensing. J. Hydrometeorol. 14, 1259–1277.

Bao, X., Zhang, F., 2013. Evaluation of NCEP–CFSR, NCEP–NCAR, ERA-Interim, and ERA-40 reanalysis datasets against independent sounding observations over the Tibetan Plateau. J. Clim. 26 (1), 206–214.

Berg, A., Lintner, B.R., Findell, K.L., Malyshev, S., Loikith, P.C., Gentine, P., 2014. Impact of soil moisture-atmosphere interactions on surface temperature distribution. J. Clim. 27, 7976–7993.

Bi, H., Ma, J., Zheng, W., Zeng, J., 2016. Comparison of soil moisture in GLDAS model simulations and in situ observations over the Tibetan Plateau. J. Geophys. Res. 121 (6), 2658–2678.

Chen, Y., Yang, K., Qin, J., Zhao, L., Tang, W., Han, M., 2013. Evaluation of AMSR-E retrievals and GLDAS simulations against observations of a soil moisture network on the central Tibetan Plateau. J. Geophys. Res. 118 (10), 4466–4475.

Deng, H.J., Pepin, N.C., Chen, Y.N., 2017. Changes of snowfall under warming in the Tibetan Plateau. J. Geophys. Res.-Atmos. 122, 7323–7341.

Feng, X., Liu, C., Rasmussen, R., Fan, G., 2014. A 10-yr climatology of Tibetan Plateau vortices with NCEP climate forecast system reanalysis. J. Appl. Meteorol. Climatol. 53 (1), 34–46.

Gao, Y.H., Li, X., Leung, L.R., Chen, D., Xu, J., 2015. Aridity changes in the Tibetan Plateau in a warming climate. Environ. Res. Lett. 10, 034013. https://doi.org/10.1088/1748-9326/10/3/034013.

Guillod, B.P., Orlowsky, B., Miralles, D.G., Teuling, A.J., Seneviratne, S.I., 2015. Reconciling spatial and temporal soil moisture effects on afternoon rainfall. Nat. Commun. 6, 6433. https://doi.org/10.1038/ncomms7443.

Hauser, M., Orth, R., Seneviratne, S.I., 2016. Role of soil moisture versus recent climate change for the 2010 heat wave in Russia. Geophys. Res. Lett. 43, 2819–2826.

Hirschi, M., Seneviratne, S.I., Alexandrov, V., Boberg, F., Boroneant, C., Christensen, O.B., Formayer, H., Orlowsky, B., Stepanek, P., 2011. Observational evidence for soil-moisture impact on hot extremes in southeastern Europe. Nat. Geosci. 4 (1), 17–21.

IPCC, 2007. Regional climate projections. IPCC Fourth Assessment Report Climate Change 2007: The Scientific Basis. Cambridge University Press, Cambridge.

Koster, R.D., Dirmeyer, P.A., Guo, Z., Bonan, G., Chan, E., Cox, P., Gordon, C.T., Kanae, S., Kowalczyk, E., Lawrence, D., Liu, P., Lu, C.H., Malyshev, S., McAvaney, B., Mitchell, K., Mocko, D., Oki, T., Oleson, K., Pitman, A., Sud, Y.C., Taylor, C.M., Verseghy, D., Vasic, R., Xue, Y., Yamada, T., Team, G.L.A.C.E., 2004. Regions of strong coupling between soil moisture and precipitation. Science 305 (5687), 1138–1140.

Koster, R.D., Schubert, S.D., Suarez, M.J., 2009. Analyzing the concurrence of meteorological droughts and warm periods, with implications for the determination of evaporative regime. J. Clim. 22 (12), 3331–3341.

Liu, Q., Fu, Y.H., Zeng, Z., Huang, M., Li, X., Piao, S., 2016. Temperature, precipitation, and insolation effects on autumn vegetation phenology in temperate China. Glob. Chang. Biol. 22 (2), 644–655.

Liu, J., Shanguan, D., Liu, S., Ding, Y., 2018. Evaluation and hydrological simulation of CMADS and CFSR reanalysis datasets in the Qinghai-Tibet Plateau. Water 10 (4), 513.

Miralles, D.G., Teuling, A.J., van Heerwaarden, C.C., de Arellano, J.V.-G., 2014. Mega-heatwave temperatures due to combined soil desiccation and atmospheric heat accumulation. Nat. Geosci. 7 (5), 345–349.

Mueller, B., Seneviratne, S.I., 2012. Hot days induced by precipitation deficits at the global scale. Proc. Natl. Acad. Sci. U. S. A. 109 (31), 12398–12403.

Saha, S., Moorthi, S., Pan, H.-L., Wu, X., Wang, J., Nadiga, S., Tripp, P., Kistler, R., Woollen, J., Behringer, D., Liu, H., Stokes, D., Grumbine, R., Gayno, G., Wang, J., Hou, Y.-T., Chuang, H.-y., Juang, H.-M.H., Sela, J., Iredell, M., Treadon, R., Kleist, D., Van Delst, P., Keyser, D., Derber, J., Ek, M., Meng, J., Wei, H., Yang, R., Lord, S., van den Dool, H., Kumar, A., Wang, W., Long, C., Chelliah, M., Xue, Y., Huang, B., Schemm, J.-K., Ebisuzaki, W., Lin, R., Xie, P., Chen, M., Zhou, S., Higgins, W., Zou, C.-Z., Liu, Q., Chen, Y., Han, Y., Cucurull, L., Reynolds, R.W., Rutledge, G., Goldberg, M., 2010. The NCEP climate forecast system reanalysis. Bull. Am. Meteorol. Soc. 91, 1015–1057. https://doi.org/10.1175/2010BAMS3001.1.

Saha, S., Moorthi, S., Wu, X., Wang, J., Nadiga, S., Tripp, P., Behringer, D., Tai, Y.-T., Chuang, H.-y., Iredell, M., Ek, M., Meng, J., Yang, R., Mendez, M.P., van den Dool, H., Zhang, Q., Wang, W., Chen, M., Becker, E., 2014. The NCEP climate forecast system version 2. J. Clim. 27, 2185–2208.

Schwingshackl, C., Hirschi, M., Seneviratne, S.I., 2017. Quantifying spatiotemporal variations of soil moisture control on surface energy balance and near-surface air temperature. J. Clim. 30 (18), 7105–7124.

Seneviratne, S.I., Lüthi, D., Litschi, M., Schär, C., 2006. Land-atmosphere coupling and climate change in Europe. Nature 443, 205–209.

Seneviratne, I.S., Corti, T., Davin, E.L., Hirschi, M., Jaeger, E.B., Lehner, I., Orlowsky, B., Teuling, A.J., 2010. Investigating soil moisture-climate interactions in a changing climate: a review. Earth Sci. Rev. 99, 125–161.

Subin, Z.M., Koven, C.D., Riley, W.J., Torn, M.S., Lawrence, D.M., Swenson, S.C., 2013. Effects of soil moisture on the responses of soil temperatures to climate change in cold regions. J. Clim. 16, 139–3158.

Taylor, C.M., de Jeu, R.A.M., Guichard, F., Harris, P.P., Dorigo, W.A., 2012. Afternoon rain more likely over drier soils. Nature 489, 423–426.

Whan, K., Zscheischler, J., Orth, R., Shongwe, M., Rahimi, M., Asare, E.O., Seneviratne, S.I., 2015. Impact of soil moisture on extreme maximum temperatures in Europe. Weather Clim. Extremes 9, 57–67.

Xie, H., Ye, J.S., Liu, X.M., E, C.Y., 2010. Warming and drying trends on the Tibetan Plateau (1971–2005). Theor. Appl. Climatol. 101 (3–4), 241–253.

Xu, Z.X., Gong, T.L., Li, J.Y., 2008. Decadal trend of climate in the Tibetan Plateau-regional temperature and precipitation. Hydrol. Process. 22, 3056–3065.

Zhang, L., Su, F., Yang, D., Hao, Z., Tong, K., 2013. Discharge regime and simulation for the upstream of major rivers over Tibetan Plateau. J. Geophys. Res. Atmos. 118 (15), 8500–8518.

Zhang, Q., Xiao, M., Singh, V.P., Liu, L., Xu, C.-Y., 2015. Observational evidence of summer precipitation deficit-temperature coupling in China. J. Geophys. Res. 120 (19), 10040–10049.

Zhang, Q., Fan, K., Sing, V.P., Sun, P., Shi, P., 2018a. Evaluation of remotely sensed and reanalysis soil moisture against in-situ observations on the Himalayan-Tibetan Plateau. J. Geophys. Res. Atmos. 123. https://doi.org/10.1029/2017JD027763.

Zhang, Q., Kong, D., Singh, V.P., Shi, P., Sun, P., 2018b. Vegetation phenology on the Qinghai-Tibetan Plateau and its response to climate change (1982–2013). Agric. For. Meteorol. 248, 408–417.

Zhao, S., He, W., Jiang, Y., 2018. Evaluation of NCEP-2 and CFSR reanalysis seasonal temperature data in China using detrended fluctuation analysis. Int. J. Climatol. 38 (1), 252–263.

Zhou, X., Geerts, B., 2013. The influence of soil moisture on the planetary boundary layer and on cumulus convection over an isolated mountain. Part I: observations. Mon. Weather Rev. 141, 1061–1078.